Monitoring the West African heat low at seasonal and intra-seasonal timescales using AMSU-A sounder

Christophe Lavaysse, Laurence Eymard, Cyrille Flamant, Fatima Karbou, M. Mimouni, A. Saci

ATMOSPHERIC SCIENCE LETTERS
Atmos. Sci. Let. **14**: 263–271 (2013)
Published online 31 July 2013 in Wiley Online Library
(wileyonlinelibrary.com) **DOI:** 10.1002/asl2.449

RMetS
Royal Meteorological Society

Monitoring the West African heat low at seasonal and intra-seasonal timescales using AMSU-A sounder

C. Lavaysse,[1,*] L. Eymard,[2] C. Flamant,[1] F. Karbou,[3] M. Mimouni[4] and A. Saci[5]

[1]*Laboratoire Atmosphère, Milieux, Observations Spatiales, CNRS and Université Pierre et Marie Curie, Paris, France*
[2]*Laboratoire d'Océanographie et du Climat: Expérimentation et Approches Numériques, IRD and Université Pierre et Marie Curie, Paris, France*
[3]*CNRM-GAME, Météo-France/CNRS, Centre d'Etude de la Neige, Saint Martin d'Heres, France*
[4]*Office National de la Météorologie, Tamanrasset, Algeria*
[5]*Office National de la Máetáeorologie, Algiers, Algeria*

*Correspondence to:
C. Lavaysse, Laboratoire Atmosphére, Milieux, Observations Spatiales, Université Pierre et Marie Curie, Paris, France.
E-mail:
christophe.lavaysse@latmos.ipsl.fr

Received: 22 October 2012
Revised: 2 May 2013
Accepted: 11 June 2013

Abstract

The Saharan heat low (SHL) is defined as a stationary thermal depression below 700 hPa located over the Sahara during the boreal summer season. This feature has a significant impact on the seasonal and intra-seasonal variability of rainfall over the Sahel. For various reasons, few observations are assimilated in operational numerical weather prediction models, especially surface sensitive observations. In this study we make use of the advanced microwave sounding unit (AMSU-A) brightness temperatures measured at 52.8 GHz (noted A4 hereafter) and at 53.6 GHz (noted A5 hereafter) to detect the heat low and to characterize its intensity at the seasonal and intra-seasonal scales. In terms of seasonal variability, AMSU-based estimates of SHL are found in good agreement with those based on the European Center Medium-range Weather Forecast ERA-I reanalyses for the period ranging from 2000 to 2011. However, differences exist between the two datasets at intraseasonal timescale. They may be related to mismatches between the numerical weather prediction model levels and the level of maximum of sensitivity of the AMSU observations. Particular meteorological situations can also explain some differences between the two types of products, as there is a lack of assimilated observations in this region. Finally, we show that the A4 brightness temperature is a suitable proxy to provide a good estimate of the location and the intensity of the SHL from daily to seasonal timescales.

Keywords: **West African monsoon; AMSU sounder; heat Low**

1. Introduction

Over the West African continent, the strength and the direction of the winds at low levels, such as the monsoon and the harmattan winds, are closely linked to surface pressure gradients. An area of high low level temperatures and low surface pressures (i.e. a heat low) has recently been shown to play an important role in shaping the low-level winds throughout the years (Lavaysse *et al.*, 2009).

In boreal summer, the West African heat low (WAHL) is generally located over the Sahara and is often referred to as the Saharan heat low (SHL). During this period, the SHL is considered to be one of the major dynamical elements of the West African monsoon system (Parker *et al.*, 2008; Lafore *et al.*, 2011). Indeed, the cyclonic circulation associated with the SHL contributes to increase both the south-westerly monsoon flow along its eastern flank and the northeasterly harmattan flow along the western flank, especially when the SHL is intense, with a well-defined low-pressure center associated with high low-level temperatures. This circulation is likely to enhance the probability of moist convection and cloud cover poleward of the main rainy zone to the east of the SHL (Knippertz, 2008; Cuesta *et al.*, 2009; Lavaysse *et al.*, 2010a; Roehrig *et al.*, 2011).

Several studies have highlighted the fact that the SHL exhibits intensity pulsations at intra-seasonal scale (Lavaysse *et al.*, 2010b; Chauvin *et al.*, 2010; Roehrig *et al.*, 2011). Such fluctuations arguably have an impact on low-level dynamics and, in turn, on moisture advection over the Sahel. Indeed, the diurnal cycle of winds (dominated by nocturnal advection) in Niamey (Niger) is correlated at synoptic and intra-seasonal timescales with the temperature to the north (i.e. in the Sahara) (Parker *et al.*, 2005), this jet is essential to bring water vapor from the south during the night (Lothon *et al.*, 2009), and the northward monsoon surges in spring occur after strong SHL episodes (Couvreux *et al.*, 2009). Furthermore, the link between the SHL intensity and the convection patterns over West Africa has been investigated during the summer season using ECMWF reanalysis and satellite data (Lavaysse *et al.*, 2010b). During extremely intense (weak) SHL events, a significant increase (decrease) of precipitation occurs over the eastern part of the Sahel. Finally, Chauvin *et al.* (2010) have identified the SHL intra-seasonal pulsations to consist of two phases, an eastern phase when the SHL is located south of the

Hoggar and a western phase when it is located over northern Mauritania.

Despite the strong influence of the WAHL on the West African monsoon system and related precipitations over the Sahel, the Sahara suffers from a sparse ground-based observational network, leading to a recurrent lack of data which can be assimilated in numerical weather prediction (NWP) models (see for example the Figure 2 of Agusti-Panareda *et al.*, 2010), thereby hindering weather forecasting or validation of climate simulations in this region.

Some recent studies have helped to improve this situation by assimilating observations, from *in situ* and from remote sensing instruments, in the NWP models (Bauer, 1999; Faccani, 2009). Following Karbou *et al.*, 2010a, 2010b, the assimilation of advanced microwave sounding unit (AMSU-A5) and water vapor channels (AMSU-B) is now performed in operational forecasting thanks to an improved land surface emissivity empirical assessment. This assimilation has a major positive impact on forecasted atmospheric fields. However, these developments, as AMSU-A5 data assimilation, are not yet used for reanalyses. These reanalyses have mainly been used so far to look at the seasonal and intra-seasonal variability of the SHL (Lavaysse *et al.*, 2009, 2010a, 2010b; Chauvin *et al.*, 2010; Roehrig *et al.*, 2011).

With this study we are looking for complementary and NWP model-independent metrics of the WAHL intensity and location using remote sensing observations not yet assimilated in NWP models. The aim of this work is also to compare results from observations and reanalysis to assess the quality of the WAHL representation using the space-borne products. The paper is organized as follows. The dataset and the method used to detect the WAHL are presented in Section 2. The characteristics of the WAHL (i.e. its intensity and location) derived from AMSU and ERA-I are presented in Section 3, together with their variability at the seasonal and the intra-seasonal timescales. Conclusions are provided in Section 4.

2. Dataset and detection methods

2.1. ERA-I reanalysis

In this study, we use 11 years of ECMWF ERA-I reanalysis (Simmons *et al.*, 2007) concomitant with the AMSU-A radiometer dataset, i.e. between 2000 and 2011. The geopotential height provided by the reanalyses is available on 37 pressure levels between 1000 and 1 hPa, with a horizontal resolution of 0.75 $\times$ 0.75. Only fields at 0600 UTC are used to detect the occurrence of the WAHL in the model. This is meant to reduce the impact of clouds and convective systems on the low-level temperature and to enable the detection of a well-defined cyclonic circulation around the WAHL (otherwise difficult to monitor because of the turbulent mixing effects in the planetary boundary layer) (Lavaysse *et al.*, 2009).

The WAHL detection using geopotential data is performed following Lavaysse *et al.*, 2009 using a criterion based on the dilatation of the lower atmosphere generated by an increase of the temperature at low-level mainly as a result of surface heating. The low-level atmospheric thickness (LLAT) is calculated between the 700 and 925 hPa geopotential heights. The WAHL is defined as the area where the LLAT exceeds a threshold defined as 90% of the thickness cumulative probability distribution function computed over the domain shown in Figure 1. The WAHL intensity (in meters) is defined as the mean atmospheric thickness within the WAHL.

2.2. AMSU data

AMSU-A sounders, flying onboard the operational NOAA polarorbiting satellites, Aqua mission, and the European Organization for the Exploitation of Meteorological Satellites (EUMETSAT) Metop A mission are designed for atmospheric temperature sensing. Over the period 2000–2011, the number of satellites carrying an AMSU instrument increased from one in 2000 to more than four after 2006. For each AMSU channel, the measured brightness temperature (noted Tb hereafter) has a maximal sensitivity at a given height, but is sensitive to the adjacent layers with a decreasing weight. In this study, channel 4 (52.8 MHz, A4 hereafter) and channel 5 (53.356 GHz, A5 hereafter) are used. While the sensitivity of A5 is maximum around 4–5 km and weak at the surface, A4 sensitivity peaks around 2 km and is also more sensitive to the surface than A5 (see Figure 1 of Eymard *et al.*, 2010). Relief effects cannot be neglected in AMSU A4 and A5 Tbs for two reasons: one is the surface temperature variation with altitude; the second is that the surface is not a black body thus angular emission variation, with respect to the local slope, may have an impact. Owing to the strong influence of the surface emission on this channel, data from the AMSU A4 are not assimilated in operational NWP systems.

AMSU-A instruments observe the Earth with a large range of zenith angles. An effect of this is the variation of observed Tb along the scan line (limb effect) due to the longer path through the atmosphere. A statistical technique, described by Eymard *et al.* (2010), was applied to adjust AMSU-A observations to nadir. Once limb adjusted, AMSU-A measurements were gridded through a time/latitude/longitude interpolation procedure. The grid resolution was chosen to be equal to $1^\circ \times 1^\circ$. As in Eymard *et al.* (2010), an interpolation method based on the Cressman weighting function algorithm (Cressman, 1959) was applied: data weight decreases with the horizontal distance and time lag with respect to the Cressman radius. To be consistent with ERA-I, and to reduce cloud contamination, only data between 0000 and 1200 UTC were used for the period from 2000 to 2011. The chosen Cressman time radius is 3 days to properly fill the domain between orbital swaths of the various satellite overpasses, and

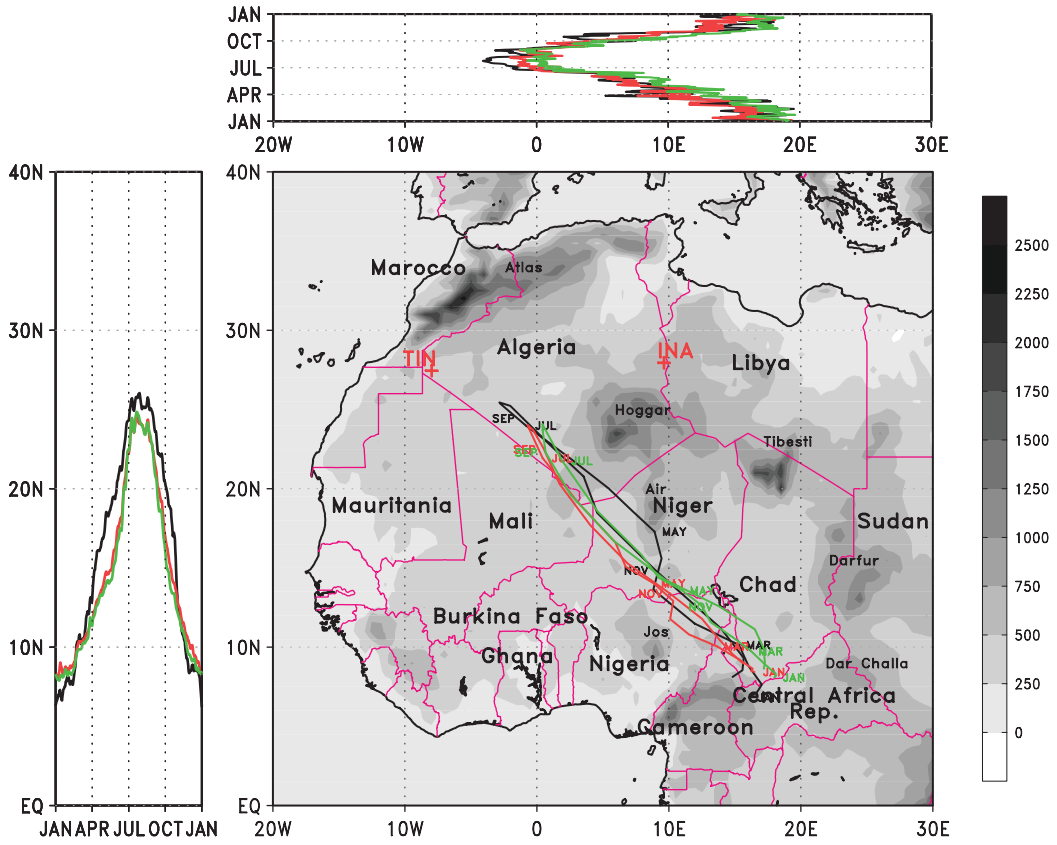

Figure 1. Seasonal evolution of the WAHL barycenter, averaged between 2000 and 2011, derived using ERA-I (black lines), AMSU-A4 (red lines) and AMSU-A5 (green lines). Top and left panels display the longitude and latitude decomposition respectively of WAHL barycenter trajectories. The gray scaling indicates the altitude (in meters). TIN and INA indicate the locations of Tindouf and In Amenas weather stations.

the chosen time interpolation step is 1 day, the grid time being 0600 UTC each day. This tends to smooth the signal but only for high frequency pulsations, approximately lower than 6 days. Note that some of the NOAA platforms are phased at around 0600 UTC, thus providing most of the final field.

Owing to the vertical weighting functions of AMSU-A5, the measured Tb is sensitive to mid-level warm air masses generated over the Arabian Peninsula which can extend spatially over Libya. These regions of mid-level warming are seen in the ERA-I reanalyses at altitudes above the 600 hPa pressure level. This results in an overestimation of detection of the WAHL from AMSU-A5 data over eastern Libya. To reduce this contamination by a signal which is not connected with the WAHL itself, the northeastern part of the domain (from 10 to 20°E and 20 to 30°N) is excluded from the WAHL detection procedure when using AMSU-A5 data. This is done by setting LLAT values to zero. As its weighting function peaks much lower in the troposphere, the WAHL detection using the AMSU-A4 data can be performed on the entire domain.

Similarly to the approach used for the ERA-I data, the WAHL derived from the AMSU observations is defined as the area where the Tb in the channel A4 or A5 exceeds a threshold defined as 90% of the Tb cumulative probability distribution function computed over the domain shown in Figure 1. As for the ERA-I data, the WAHL intensity (in K) is defined as the mean Tb over grid points where the WAHL has been detected.

3. Results

3.1. Seasonal cycle

3.1.1. WAHL location

In this section, the seasonal cycle of the WAHL barycenter defined using the reanalysis and satellite observations are compared (Figure 1).

In winter (December to March), the WAHL barycenter locations derived from AMSU A4 and A5 channels as well as from ERA-I are in fair agreement and lie over southern Chad. Likewise, in summer (July to September), the barycenter positions are found over Southern Algeria, but the WAHL derived from ERA-I positioned to the northwest of the WAHL detected with AMSU. These winter and summer locations occurring in regions of low topography were identified as being stable positions by Lavaysse *et al.* (2009).

During the spring and fall seasons, the WAHL barycenter trajectories from the three datasets slightly differ. The WAHL barycenter derived from ERA-I takes the most northeastern route, closer to the Air and

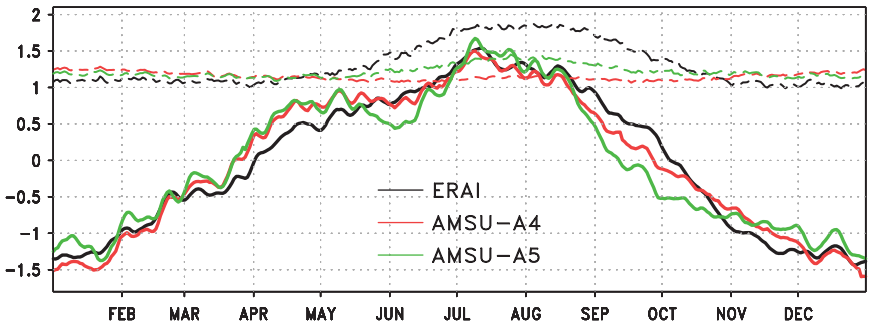

Figure 2. Seasonal evolution of the WAHL intensity (solid lines) and standardized seasonal intensity with respect to the averaged daily thickness and standard deviation of the thickness over the domain (see text for more details, dashed lines), averaged throughout the 2000–2011 period, using ERA-I (black lines), AMSU-A4 (red lines) and AMSU-A5 (green lines).

Hoggar Mountains. The slightly more western route taken by the AMSU-A4-derived WAHL with respect to that derived from AMSU-A5 may be explained by the different weighting functions.

It should be noted that the difference between the WAHL seasonal cycles derived from ERA-I and AMSU data is not affected by the number of satellites. Even in 2000, when only one platform is available, a good overall agreement is found between the seasonal cycle of the AMSU-derived WAHL and the one derived using ERA-I.

3.1.2. WAHL intensity

The seasonal evolutions of the normalized WAHL intensity, with respect to the average and the standard deviation of these intensities, are compared in Figure 2, solid lines.

During the intensification phase, the AMSU-derived WAHL is more intense (i.e. deeper) than the WAHL derived from ERA-I in April and during the first 2 weeks of May. The phase of maximum WAHL intensity is in good agreement for all datasets. Large differences are noticeable during the WAHL retreat phase. AMSU A4 and A5 values being weaker than their ERA-I one in September.

The spatially normalized WAHL intensity with respect to surrounding areas is a proxy for the local intensification of the WAHL activity compared to its environment and is shown Figure 2 (dashed lines). This normalization has been performed as follows:

$$x' = \frac{\overline{x} - \overline{X}}{\sigma_X}$$

where $\overline{x}$ represents the mean Tb or LLAT within the WAHL, $\overline{X}$ the mean and σ_X the standard deviation of Tb or LLAT over the entire domain.

The temperature anomaly increase within the WAHL that contributes to enhance the horizontal circulation generated by the low-pressure area. As observed by Lavaysse *et al.* (2009), the relative ERA-I-derived WAHL intensity tends to increase during the summer period, with a maximum in July and August (values larger than 1.8). The time evolution from AMSU-A5 WAHL also presents an increase during the same period, but the intensification is less pronounced (below 1.5) than for ERA-I. Finally using AMSU-A4, there is no relative intensification of the WAHL observed during the period of interest because of an increase of both the mean Tb and its standard deviation in summer.

The local enhancement of the WAHL intensity is especially underestimated in AMSU-A4. These differences are associated with the larger summer increase of the average of Tb than LLAT over the entire domain in relation to the average value within the WAHL (not shown).

Nevertheless, the relative good agreement between WAHL location and intensity from ERA-I, AMSU-A4 and AMSU-A5 suggests that these independent products can be further used to detect and characterize the WAHL at seasonal timescale. Only the summer relative enhancement, which is different in each product used, is still not well understood.

3.2. The Saharan heat low period

As detailed in Lavaysse *et al.* (2009), the second component of the empirical orthogonal function (EOF) of the yearly WAHL location can be used to define the beginning and the end of the stationary location of the SHL. This information is relevant for determining the beginning and the end of the period of so-called established monsoon (Sultan and Janicot, 2000).

The same methodology was applied to the WAHL detection derived from ERA-I and AMSU during the 2000–2011 period. The second component explains 24,18 and 16% of the total variance for ERA-I, AMSU-A4 and AMSU-A5, respectively. The maximum of this pattern is located in western Algeria (around 5°W, 27°N). It represents the stationary location of the WAHL during the summer season over the Sahara. It is consistent with the one obtained by Figure 10c in Lavaysse *et al.* (2009) over a longer period with ERA40 reanalyses. On the basis of the time evolution of the second EOF eigenvalues, the ERA-I-derived beginning date of the established SHL is 19 June ± 7 days, in good agreement with ERA40 derived date over the 1979–2001 period [the 20 June ± 10 days (Lavaysse *et al.*, 2009)]. Using AMSU, the SHL period

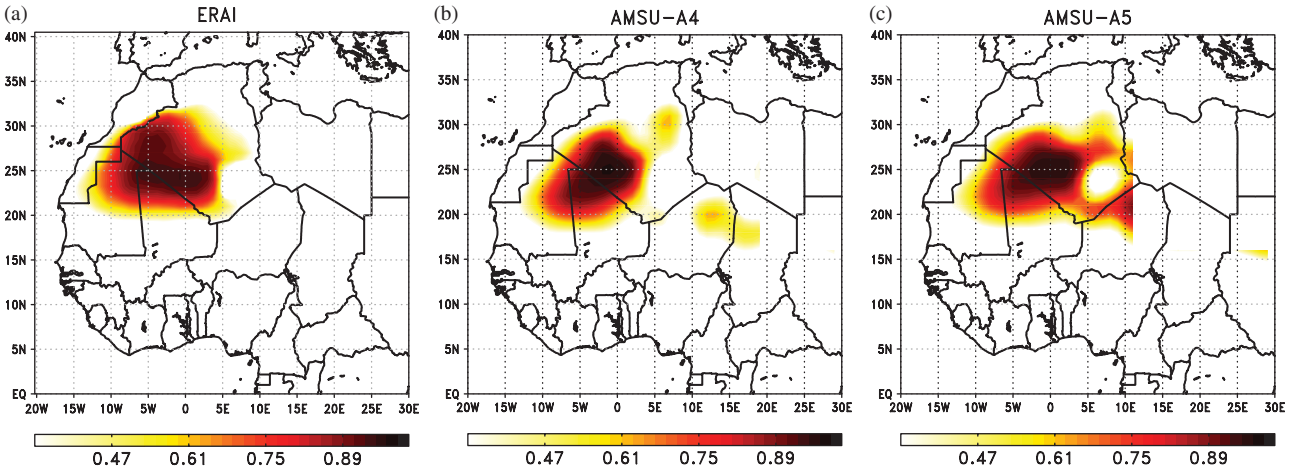

Figure 3. Mean occurrence probability of the SHL in summer (July to August), averaged between 2000 and 2011, using (a) ERA-I, (b) Tb from AMSU-A4 and (c) Tb from AMSU-A5.

starts the 18 June ±5 days on the basis of A4 and 14 June ±7 days based on A5. The average ending date for the SHL based on ERA-I is 19 September ±9 days, i.e. 2 days later than found using ERA40 (Lavaysse *et al.*, 2009). Using the AMSU products, the ending date for the SHL is found slightly later: 23 September ±5 days and 24 September ±3 days, for A4 and A5, respectively. Considering the uncertainty range on each date determination, all products are in fair agreement, with possibly a few days lag for the A5 beginning date.

During the established monsoon period, the mean occurrence probability of the SHL (defined as the mean probability of detecting the SHL over each grid point) derived from ERA-I is in agreement with that derived from the AMSU products (Figure 3). Nevertheless, differences appear in mountainous regions, especially over the Hoggar and Atlas Mountains, with a larger occurrence probability of the AMSU-derived SHL detected over the low lands rather than higher reliefs.

The main reason for this discrepancy is probably related to the weighting function differences for ERA-I and AMSU. In the ERA-I case, an equal weight is given to all tropospheric temperatures between 925 and 700 hPa. On the contrary, the AMSU A4 peaks around 850 hPa and AMSU A5 around 700 hPa. Similarly, the three products do not therefore monitor the lower troposphere. An additional possible origin of these differences could be an underestimation of the radiative cooling during the night in the ERA-I (Miller *et al.*, 2012).

3.3. Intra-seasonal SHL pulsations

In this section we compare intra-seasonal pulsations as derived from ERA-I and AMSU using EOF and the LLAT methods. The method based on the LLAT has already been used to study intra-seasonal pulsations of the WAHL (Lavaysse *et al.*, 2010a). We focus on the SHL period, i.e. 90 days from 20 June to 17 September. We selected the period from 2007 to 2011, during which several AMSU instruments were in orbit. The reason is that a minimum number of satellites are necessary to properly characterize the intraseasonal variations. Before 2007, when less than our platforms are in orbit, large discrepancies between AMSU and ERA-I variation patterns are observed that are closely linked to missing data over the Sahara between two satellite swaths. After 2007, at least four platforms are in orbit and the agreement between ERA-I and AMSU A4 is stable with time. Owing to the potential contamination of the AMSU-A5 observations by warm air masses over Libya, and the better representation of the WAHL at seasonal timescale using AMSU-A4, only metrics derived from AMSU-A4 are compared with those derived from ERA-I in this section. The scatter plot of the normalized SHL intensity derived from AMSU A4 *versus* the SHL intensity determined from ERA-I underlines the good agreement between the two datasets (correlation of 0.82, Figure 4).

Owing to the scarcity of observations, the characterization of the intra-seasonal pulsations of the WAHL is a challenge, as it requires good descriptions of the temperature fields over the entire Sahara. The representations of these pulsations are compared using EOF analyses for different sets of data. First, EOF analysis is performed on the data after applying a 25-day high band pass filter over the entire domain on the LLAT and A4 Tb in order to grasp the intra-seasonal variability pulsations as done in Chauvin *et al.* (2010). The first EOF pattern obtained (explaining 19% of the total variance) is shown in Figure 5(a). This result agrees with Chauvin *et al.* (2010). The same analysis performed using the 25-day high band pass filter of Tb from AMSU-A4 (Figure 5(b)) explains 16% of the total variance. The east–west pulsation pattern of the WAHL is centered over 0°E in both datasets. The main difference is the largest sensitivity of the Tb over the continent that tends to increase the variability signal over the southern part of Libya. As the method derived from Chauvin *et al.* (2010) displays

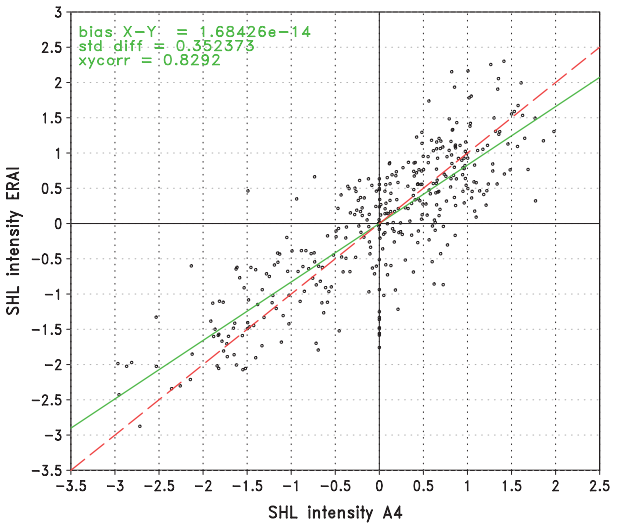

Figure 4. Scatter plot between the mean normalized intensity of the SHL derived from ERA-I (*y*-axis) and AMSU-A4 (*x*-axis) during established SHL phase (see text for more details). A linear regression has been added (green lines) and the characteristics of the distribution are indicated (top left), respectively the bias, the standard deviation and the temporal correlation.

the anomaly of temperature fields, it does not provide exactly the pulsation of the WAHL which is associated with the largest temperature or thickness area. Another EOF analysis was therefore performed using the products derived from the WAHL location method. In this case, the analysis is performed only over areas detected and tracked as WAHL during the season. We focus on the WAHL pulsation itself. The first EOF component is associated with the WAHL at seasonal cycle (not shown). The patterns of the second component, which explain 12 and 16% for ERA-I and AMSU-A4 respectively, depict a clear east–west displacement of the WAHL area during the summer season in both products (Figure 5(c) and (d)). The southern location of these pulsations with respect to features in Figure 5(a) and (b) is explained by the difference in the method used, focusing on the WAHL location in summer. The slight different locations of the pulsation center between ERA-I and AMSU-A4 can be explained by the A4 Tb sensitivity to the surface temperature, lower in the Hoggar Mountains, as well as possible relief effects on the measurements. However, a positive bias in the ERA-I atmospheric temperature in the Hoggar is not fully excluded as well.

The temporal evolution of the eigenvalues associated with the pattern shown Figure 5(a) and (b) is displayed in Figure 6(a), showing short-scale pulsations lower than 25 days. As neither ERA-I nor AMSU-A4 WAHL signature can be taken as a reference, we attempt to compare the temporal evolution of their eigenvalues with those derived from time series of two weather station data located in Algeria, namely Tindouf and In Amenas (see locations in Figure 1). These stations were selected for their respective locations: they are implemented at roughly the same latitude and on either side of the mean WAHL location, i.e. in the eastern or western phase of the SHL as shown in Figure 5. After filtering out period longer than 25 days, the temporal evolution of the 2-m temperature is plotted in Figure 6(b). The temperature difference between the two stations can be considered as a proxy for the SHL phase (positive gray bars indicating an eastern phase of the SHL) assuming a good correlation between the 2-m temperature and 850 hPa temperature field (which is a realistic approximation most of the time). The opposite phase between the time series of two stations confirms that surface temperatures are acquired in different phases of the WAHL at intra-seasonal timescales. Despite the assimilation of these observations in the reanalyses, the correlation between the eigenvalues of the WAHL location derived from ERA-I (black line in Figure 6(a)) and from the observations (gray bars in Figure 6(b)) is lower than 0.5. The same comparison with the one derived from the AMSU-A4 Tbs over the entire domain shows no correlation.

The same temporal evolution based on the SHL eigenvalue from EOF shown Figure 5(c) and (d) is shown Figure 6(c). The signal is not high-pass filter and shows an influence of the seasonal cycle with a clear eastern anomaly at the beginning and at the end of each summer season. There is also an impact of the Atlantic sea-surface temperature that tends to reduce the detection and variability of the WAHL using AMSU-A4 over the Western part of the Sahara.

The correlation of the stations SHL variation (gray bars in Figure 6(b)) is still found with the evolution of the HL phase using the EOF of the HL location derived from ERA-I (black line in Figure 3(c), $r^2 = 0.35$), but these agreements are lower than using the entire fields of LLAT (as shown in Figure 6(a)). This could be explained by the assimilation of the data from these stations in the reanalysis and the filtering method used in the first method. Nevertheless, these products are complementary and could reflect different characteristics according to the method used. For example, at the end of summer season 2009, the evolution of the filtered LLAT signal (black line in Figure 6(a)) reflects a east–west pulsations, whereas the WAHL detection derived from ERA-I (black line in Figure 6(c)) detects a WAHL to the east, due to an earlier end of the summer season.

4. Discussions and conclusions

This study presents the first investigation of the WAHL characteristics at seasonal timescales based on satellite observations. An attempt is also made to assess the intra-seasonal variability of the SHL in a region (i.e. the Sahara) where observations are scarce and accurate weather forecasting is vital due to the influence of the SHL on convective activity over the Sahel.

Heat low characteristics from ERA-I geopotential height reanalyses and Tb observations (channels A4

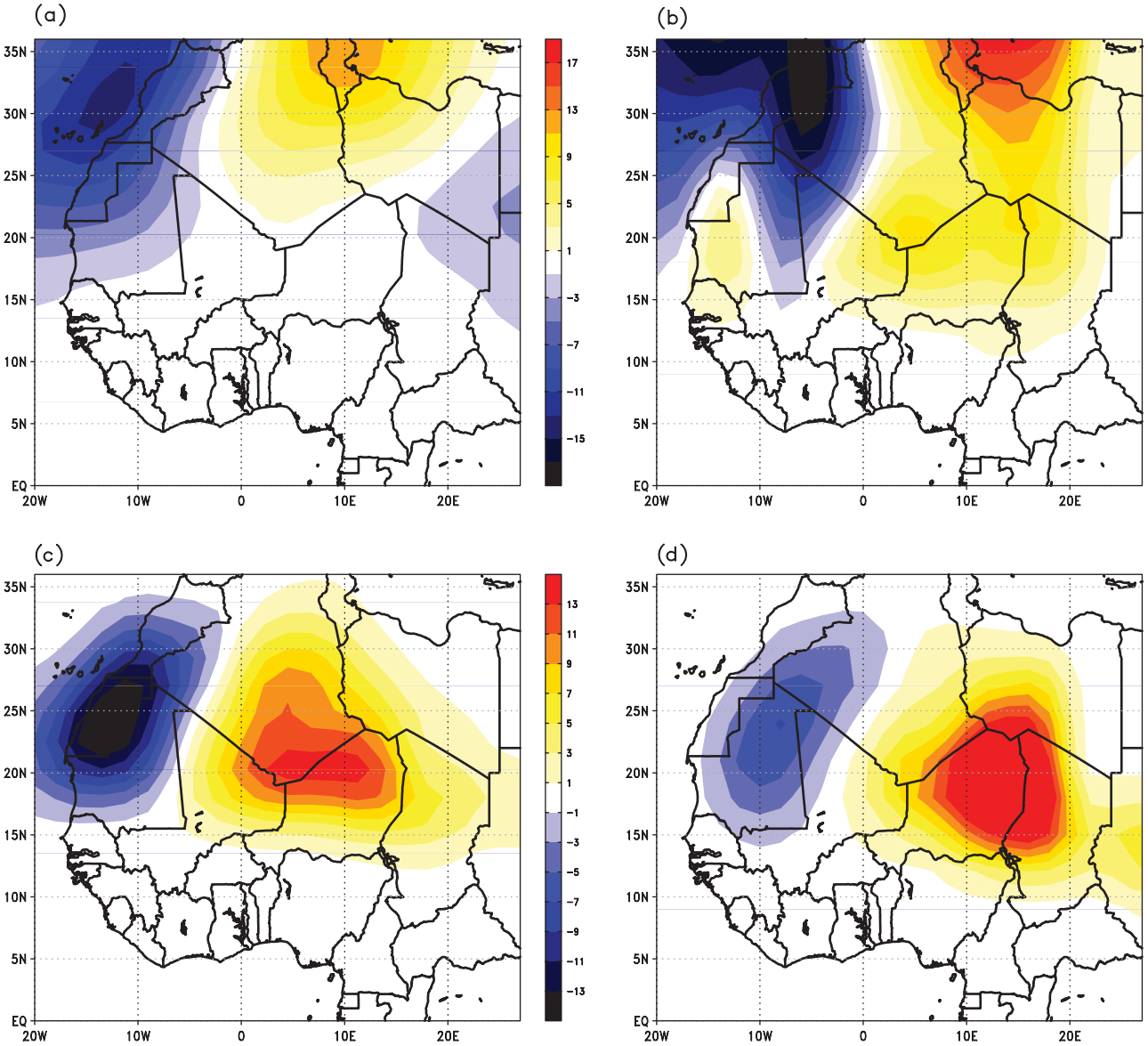

Figure 5. (a) Pattern of the first EOF, that explained 19% of the total variance, of the 25 day high band pass filter of the LLAT (see text for more details) derived from ERA-I (in meters). (b) Same as (a) but for the Tb derived from AMSU-A4 that explains 16% of the total variance. EOF of the HL location, based on the LLAT detection method (see text for more details), which explain 12 and 16% of the total variance using ERA-I (c) and AMSU-A4 (d) respectively.

and A5) from the AMSU radiometer are found to be in good agreement at seasonal timescale in terms of WAHL location and intensity. The trajectories of the WAHL barycenter in spring and fall display a more southern route when derived using AMSU-A4 because of the low surface temperature over the orography (Air and Hoggar Mountains). This is especially marked for channel 4 that is more sensitive to the surface temperature. In summer, the SHL intensity derived from ERA-I shows a increase with respect to the surrounded areas, which is not well observed in the AMSU products.

At intra-seasonal timescale, pulsations of the SHL intensity derived from AMSU and ERA-I are in good agreement. Also, the longitudinal location of the SHL was found in broad agreement between ERA-I and AMSU. Nevertheless, differences are observed and may be related to specific meteorological conditions associated with cold Atlantic air inflows into the Sahara. An in-depth study should also be conducted on the ability of the AMSU product to display the so-called monsoon jump period, defined as the beginning of the rainy season over the Sahel. To perform this study a longer AMSU observational dataset length is necessary. In this study, we have seen that there is a better agreement between the ERA-I and AMSU intra-seasonal characteristics after 2007 when the data from more than four satellites are used. This is associated with the significant increase in the spatial coverage by the space-borne instruments over the Sahara.

In conclusion, the agreement between two NWP model-independent WAHL metrics derived from AMSU-A at the seasonal timescale and their ERA-I-derived counterparts allows concluding about the good

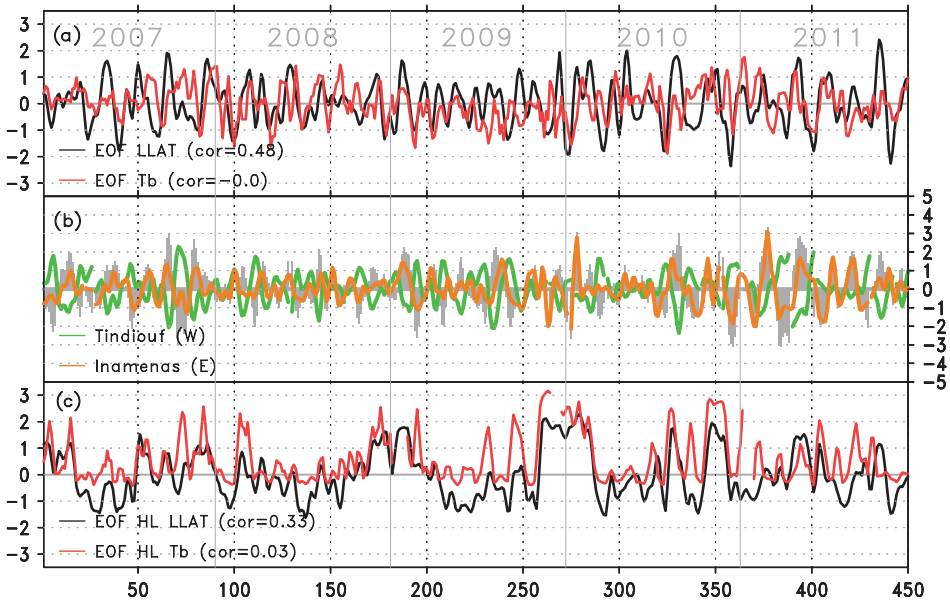

Figure 6. (a) Temporal evolution of the two eigenvalues, associated with the patterns displayed in Figure 5(a) and (b), during the summer period (20 June to 17 September) from 2007 to 2011 (450 days) from ERA-I (black line) and AMSU-A4 (red line). (b) Temporal evolution of the 2-m temperature with 25 day high band pass filter at Tindouf (Algeria, green line) and In Amenas (Algeria, orange line) and difference between the two stations (gray bars). (c) Same as (a) using the HL location (associated with patterns in Figure 5(c) and (d)). Positive values of the lines in (a) and (c) and positive values for the bars in (b) are associated with an eastern position of the HL. Temporal correlation between each eigenvalues and the observed temperature difference are indicated in (a) and (c). Vertical dashed lines separate each summer season.

representation of the WAHL characteristics in ERA-I. Moreover, the use of the Tb from AMSU-A4 appears also to be appropriate to detect and characterize the WAHL seasonal and intra-seasonal variability. This is the first time that an observational, NWP-independent (because not assimilated) dataset is used to assess the WAHL characteristics issued from NWP models. We consider that the use of the Tb from AMSU-A4 is suitable to provide an accurate estimate of the intensity of the SHL and may be used as a near-real time product to contribute to the monitoring of the West African monsoon system. There are more uncertainties about the location of the WAHL and the east/west phases of the WAHL. This could be due to different reasons: (1) the different weighing function between the two products, (2) the relative short period of the analysis (only 5 years) and (3) the model or the observation errors. The temporal evolution from ERA-I seems to be more in accordance with the evolution of the surface stations, but this agreement is likely due to the fact that the data from these stations are assimilated in reanalysis.

Further work is still needed. In particular, it will be useful to compare A4 observations with Tb simulations using ERA-I reanalysis profiles as inputs to a radiative transfer model in order to better understand the differences highlighted between the model-based and observation-based SHL characteristics. The RTTOV model (Matricardi *et al.*, 2004; Saunders *et al.*, 1999) will be used for that purpose in combination with *in situ* observations, satellite products and airborne measurements acquired over the Central Sahara during the recent FENNEC campaign which took place in June 2011 (Washington *et al.*, 2012).

References

Agusti-Panareda A, Beljaars A, Ahlgrimm M, Balsamo G, Bock O, Forbes R, Ghelli A, Guichard F, Köhler M, Meynadier R, Morcrette J-J. 2010. The ECMWF re-analysis for the AMMA observational campaign. *Quarterly Journal of the Royal Meteorological Society* **136**: 1457–1472.

Bauer P. 1999. 4D-Var assimilation of MERIS total column water-vapour retrievals over land. *Quarterly Journal of the Royal Meteorological Society* **135**: 1852–1862.

Chauvin F, Roehrig R, Lafore J-P. 2010. Intraseasonal variability of the Saharan heat low and its link with mid-latitudes. *Journal of Climate* **23**: 2544–2561.

Couvreux F, Guichard F, Bock O, Campistron B, Lafore J-P, Redelseperger J-L. 2009. Synoptic variability of the monsoon flux over West Africa prior to the onset. *Quarterly Journal of the Royal Meteorological Society* **136**: 414–432. DOI: 10.1002/qj.473.

Cressman GP. 1959. An operational objective analysis system. *Monthly Weather Review* **87**: 367–374.

Cuesta J, Lavaysse C, Flamant C, Mimouni M, Knippertz P. 2009. Northward burst of the West African monsoon and interactions with large-scale conditions leading to rainfall over the Hoggar Massif, Algeria. *Quarterly Journal of the Royal Meteorological Society* **10**: 34–42.

Eymard L, Karbou F, Janicot S, Chouaib N, Pinsard F. 2010. On the use of advanced microwave sounding unit-a and -b measurements for studying the monsoon variability over West Africa. *Journal of Geophysical Research* **115**. DOI: 10.1029/2009JD012935.

Faccani C, Rabier F, Fourrié N, Agusti-Panareda A, Karbou F, Moll P, Lafore J-P, Nuret M, Hdidou F, Bock O. 2009. The impact of the AMMA radiosonde data on the French global assimilation and forecast system. *Weather and Forecasting* **24**: 1268–1286.

Karbou F, Gérard E, Rabier F. 2010a. Global 4D-Var assimilation and forecast experiments using AMSU observations over land. Part-I:

Impact of various land surface emissivity parameterizations. *Weather and Forecasting* **25**: 5–19. DOI: 10.1175/2009WAF2222243.1.

Karbou F, Rabier F, Lafore J-P, Redelsperger J-L, Bock O. 2010b. Global 4D-Var assimilation and forecast experiments using AMSU observations over land. Part II: Impact of assimilating surface sensitive channels on the African monsoon during AMMA. *Weather and Forecasting* **25**: 20–36. DOI: 10.1175/2009WAF2222244.1.

Knippertz P. 2008. Dust mobilization in the West African heat trough - the role of the diurnal cycle and of extratropical synoptic disturbances. *Meteorologische Zeitschrift* **17**(5): 553–563.

Lafore JP, Flamant C, Guichard F, Parker DJ, Bouniol D, Fink A, Giraud V, Gosset M, Hall N, Höller H, Jones SC, Protat A, Roca R, Roux F, Sard F, Thorncroft C. 2011. Progress in understanding of weather systems in West Africa. *Atmospheric Science Letters* **12**: 7–12.

Lavaysse C, Flamant C, Janicot S, Parker DJ, Lafore J-P, Sultan B. 2009. Seasonal evolution of the West African heat low, a climatological perspective. *Climate Dynamics* **33**. DOI: 10.1007/s00382–009–0553–4.

Lavaysse C, Flamant C, Janicot S. 2010a. Regional scale convection patterns during strong and weak phases of the Saharan heat low. *Atmospheric Science Letters* **11**: 255–264. DOI: 10.1002/asl2.284.

Lavaysse C, Flamant C, Janicot S, Knippertz P. 2010b. Links between African easterly waves, midlatitude circulation and intraseasonal pulsations of the West African heat low. *Quarterly Journal of the Royal Meteorological Society* **136**: 141–158. DOI: 10.1002/qj.555.

Lothon M, Said F, Lohou F, Campistron B. 2009. Observation of the diurnal cycle in the low troposphere of West Africa. *Monthly Weather Review* **136**: 3477–3500.

Matricardi M, Chevallier F, Kelly G, Thépaut JN. 2004. An improved general fast radiative transfer model for the assimilation of radiance observations. *Quarterly Journal of the Royal Meteorological Society* **130**: 153–173.

Miller MA, Virendra P, Ghate P, Zahn R. 2012. The radiation budget of the West African Sahel and its controls: a perspective from observations and global climate models. *Journal of Climate* **25**: 5976–5996. DOI: 10.1175/JCLI–D–11–00072.1.

Parker DJ, Thorncroft CD, Burton R, Diongue-Niang A. 2005. Analysis of the African easterly jet, using aircraft observations from the JET 2000 experiment. *Quarterly Journal of the Royal Meteorological Society* **131**: 1461–1482.

Parker DJ, Fink A, Janicot S, Ngamini JB, Douglas M, Afiesimama E, Agusti-Panareda A, Beljaars A, Dide F, Diedhiou A, Lebel T, Polcher J, Redelsperger JL, Thorncroft CD, Wilson GA. 2008. The AMMA radiosonde program and its applications for the future of atmospheric monitoring over Africa. *Bulletin of the American Meteorological Society* **89**: 1015–1027.

Roehrig R, Chauvin F, Lafore J-P. 2011. 10–25-day intraseasonal variability of convection over the Sahel: A role of the Saharan heat low and midlatitudes. *Journal of Climate* **24**: 5863–5878.

Saunders RW, Matricardi M, Brunel P. 1999. An improved fast radiative transfer model for assimilation of satellite radiance observations. *Quarterly Journal of the Royal Meteorological Society* **125**: 1407–1425.

Simmons A, Uppala S, Dee D, Kobayashi S. 2007. ERA-interim: new ECMWF reanalysis products from 1989 onwards. *ECMWF Newsletter* **110**: 25–35.

Sultan B, Janicot S. 2000. Abrupt shift of the ITCZ over West Africa and intra-seasonal variability. *Geophysical Research Letters* **27**(20): 3353–3356.

Washington R, Parker DJ, Marsham JH, McQuaid J, Brindley H, Todd MC, Highwood EJ, Flamant C, Chaboureau J-P, Kocha C, Saci A, Bechir M. Fennec - the Saharan climate system: an overview. EGU Meeting 2012, Vienna, Austria, 23–27, April 2012.

